Extraction and interpretation of ring structures in images of biological hard tissues: application to fish age and growth estimation.

Ronan Fablet

EXTRACTION ADN INTERPRETATION OF RING STRUCTURES IN IMAGES OF BIOLOGICAL HARD TISSUES: APPLICATION TO FISH AGE AND GROWTH ESTIMATION

Ronan Fablet

IFREMER/LASAA

BP 70, 29280 Plouzane,France

ABSTRACT

This paper presents a general framework for the automated estimation of age and growth from images of biological materials depicting concentric ring-like structures such as tree trunks, corals, bivalve seashells, fish scales or otoliths. This interpretation task can be seen as a ring segmentation issue, where growth rings are associated to image ridge and valley structures. This is stated as the Bayesian selection of a subset of partial ring curves extracted using a semi-local template-based growth-adapted scheme. The application to fish otolith interpretation provides a consistent and convincing validation of the proposed framework.

1. PROBLEM STATEMENT AND RELATED WORK

Age and growth data acquired from the analysis of ring-like structures in biological hard tissues (fish otoliths, shells of sea shells, tree trunks, corals,...) are key information for a broad range of scientific issues such as marine stock assessments, marine ecology, paleoclimatology or archeology. We provide examples of such images involving ring-like structures in Fig.1 and in Fig.4. The deposit of ring structures is mostly periodic (mainly seasonal or daily depending). Counting growth rings then leads to an estimation of the age, whereas growth increments can be estimated from the distance between successive rings. Since large collections of biological data are needed (typically, several thousands of samples per year for fish stock assessment), computer-aided tools [8] are being sought. Our work is dedicated to the automation of age and growth estimation from the analysis of images of biological hard tissues. The key issues, as illustrated in Fig.1, lie in the use of growth information both to design a robust ring extraction framework taking into account growth non-linearity, and to discriminate actual growth rings from irrelevant ones. Previous work [5, 9, 10] has mainly focused on the information extraction step but have not tackled the actual interpretation task. The latter is a complex issue as stressed by the the results of the European workshop on plaice otolith interpretation held in 2003: inter-reader agreement rates vary from 40% to 95% depending on readers' experience, whereas this rate is comprised between 85% and 95% for expert readers. As a first step, statistical learning has been recently investigated for automating age estimating from a training set of samples interpreted by experts [4]. However, this approach is limited to age estimation and cannot be straightforwardly extended to growth ring extraction and growth estimation.

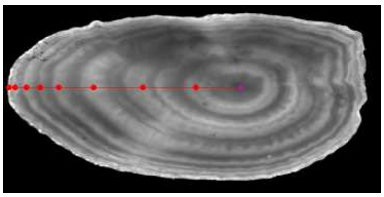

Fig. 1. *Example of growth ring structures observed on a plaice otolith illustrating the complexity of the interpretation of growth rings due to the presence of false rings (eg, between the first and second rings), and to the non-linearity of the associated growth pattern (the last two rings tend to be closer and hard to distinguish). The positions of actual growth rings are depicted by the markers set on the radial drawn from the otolith center to the edge.*

A two-stage approach is proposed to bring new solutions to these issues. A semi-local growth-adapted template-based scheme is first developed to robustly extract meaningful partial ring curves curves. Second, exploiting *a priori* growth information provided by a set of samples interpreted by an expert, the interpretation step is viewed as a Bayesian selection of a subset of the extracted curves. The subsequent is organized as follows. Sections 2 detail the semi-local approach proposed for the segmentation of partial 2D ring curves. The application to age and growth estimation is discussed in Section 3. Results are presented in Section 4.

2. EXTRACTION OF PARTIAL RING CURVES

2.1. Semi-local template-based framework

The first stage of our approach relies on the extraction of partial ring segments. As a result of the accretionary process leading to the formation of the hard tissues, the alternated

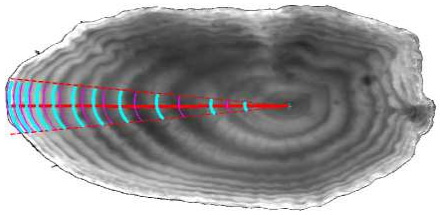

Fig. 2. *Local template-based scheme for the detection of elementary ring segments*

translucent and opaque rings are rather concentric w.r.t. the growth center, and ring shapes can often roughly be approximated (at least locally) as scaled versions of a given template. Rather than exploring purely local techniques for ridge and valley detection [2, 7], we then prefer investigating the use of the external shape as the parametric model of ridge and valley structures, and we extend the global template approach presented in [9] to a semi-local framework.

The extraction of local elementary ridge or valley segments illustrated in Fig.2 proceeds as follows. Given a set of overlapping angular sectors defined w.r.t. the known growth center, we aim at determining within each angular sector the scaling factors, such that the scaled local template approximately fits the local ridge and valley segments. This is stated as the computation of the zero crossings of the first-order derivative of the the median intensity along the scaled template. Let us stress that the computation of these derivatives needs to account for the time-frequency features of hard tissue due to the decrease in the width of the growth rings when the hard tissue gets older. To cope with this issue, we use a demodulation scheme w.r.t. a mean *a priori* growth pattern learned from training samples.

2.2. Extraction of 2D ridge and valley curves

Given the set of extracted elementary ridge and valley segments, we aim at merging these elementary segments to form meaningful curves. Numerous perceptual grouping algorithms have been developed to extract curves from candidate points or elementary segments [1, 6]. These techniques rely on general geometric criteria such as good continuations [1] or curve smoothness [6]. When dealing with the analysis of growth rings within hard tissue images, three geometric features are of key interest: the growth rings are concentric; there is an alternation of opaque and translucent rings; opaque and translucent rings never cross each other.

The proposed grouping procedure exploits these features. More precisely, it proceeds as follows for elementary ridge segments (and, conversely for valley ring structures). For a given pair of elementary ridge segments associated to two neighboring angular sectors, the decision rule used to merge this pair of segments evaluates whether or not elementary valley segments within the neighboring angular sectors lie

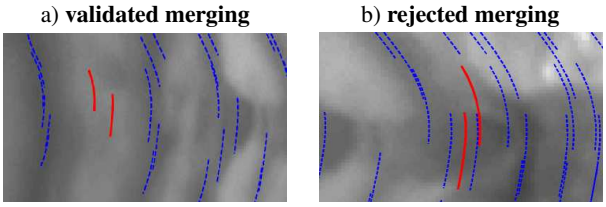

Fig. 3. *Decision rule for merging a pair of neighboring elementary ridge segments: a) validated merging, b) rejected merging. The pair of tested segments is displayed by a solid line, and neighboring elementary valley segments by dashed lines.*

between the pair of tested segments in terms of distance to the growth center. Fig.3 illustrates this decision rule for two cases: one where the merging is validated and the other one where it is rejected. A ridge curve is finally formed by the set of elementary ridge segments which can be linked by a path going through merged segments.

3. IMAGE INTERPRETATION FOR AGE AND GROWTH ESTIMATION

From a set of partial ring curves, the actual interpretation of the image content in terms of age and growth estimation comes to the selection of a curve subset corresponding to the actual growth rings. One should point out that several curve subsets might correspond to the correct interpretation, since an actual growth ring might be covered by several partial curves. Besides, some detected curves might not correspond to actual rings, but to false rings or might be due to noise patterns. To achieve this interpretation task, we rely on the protocols followed by expert readers. Mainly, it involves three different aspects: first, the detection of candidate ring-like structures; second, the evaluation of the significativity of any possible rings w.r.t. length and contrast information; third, the analysis of the spacial arrangement of the validated ring structures, which needs both to correspond to an alternation of translucent and opaque rings, and to conform to some *a priori* growth features.

To take off these protocols, the selection of a relevant curve subset is stated as a Bayesian labeling issue, where a binary label, "selected" or "rejected" is assigned to each extracted ridge or valley curve. Let us denote by $\mathcal{C}$ the set of extracted ridge and valley curves as described in the previous section. This set is sorted w.r.t. the distance between ring curves and the growth center (the computation of this distance needs to be direction-invariant ans is normalized w.r.t. the distance along the main reading axis). Let us also define $\mathcal{L}$ the binary label set {"selected", "rejected"}, $e_{\mathcal{C}}$ the set of labels $\{e_c\}_{c\in\mathcal{C}}$ for a given labeling configuration, $o_{\mathcal{C}} = \{o_c\}_{c\in\mathcal{C}}$ the features computed for all ring curves $c \in \mathcal{C}$ to evaluate their significativity. The selection of the relevant curve subset then comes to retrieve the best labeling configuration $\hat{e}_{\mathcal{C}}$ maximizing the MAP crite-

rion: $\hat{e}_{\mathcal{C}} = \arg \max_{e_{\mathcal{C}} \in \mathcal{L}^{|\mathcal{C}|}} P(o_{\mathcal{C}}|e_{\mathcal{C}})P(e_{\mathcal{C}})$, where $P(o_{\mathcal{C}}|e_{\mathcal{C}})$ is the data-driven term and $P(e_{\mathcal{C}})$ integrates an *a priori* knowledge on growth variability.

The data-driven likelihood $P(o_{\mathcal{C}}|e_{\mathcal{C}})$ is intended to evaluate the significativity of each ring curve given a labeling configuration $e_{\mathcal{C}}$: $P(o_{\mathcal{C}}|e_{\mathcal{C}}) = \prod_{c \in \mathcal{C}} P(o_c|e_c)$. As previously mentioned, experts mainly rely on the perception of contrast and ring continuity. Since contrast information is already implicitly used to extract ring curves, the likelihood $P(o_c|e_c)$ is defined from the angular length L_c of the curve c. Using an energy setting, $P(o_c|e_c)$ is expressed as: $P(o_c|e_c) \propto exp[-U_1(L_c, e_c)]$. The energy function U_1 is designed to favor the selection of ridge and valley curves with a large length value:

$$\begin{cases} U_1(L_c, e_c) = 1 - s_1(L_c - \nu_1), & \text{if } e_c = \text{“selected”} \\ U_1(L_c, e_c) = s_1(L_c - \nu_1), & \text{if } e_c = \text{“rejected”} \end{cases},$$

where $s_1()$ is a smooth step function rescaled between 0 and 1 and ν the length threshold. This parameter value is easy to set since it simply expresses from which length value a ring curve is regarded as visually significant.

In order to explicitly define the *a priori* term $P(e_{\mathcal{C}})$, we further introduce $g_{e_{\mathcal{C}}}$ the growth pattern associated to the label configuration $e_{\mathcal{C}}$ (i.e., the growth pattern computed for the selected ring curves $S(e_{\mathcal{C}})\{c^* \in \mathcal{C}/e_{c^*} = selected\}$). $P(e_{\mathcal{C}})$ is then evaluated as the likelihood that the growth pattern $g_{e_{\mathcal{C}}}$ is relevant w.r.t. *a priori* growth information: $P(e_{\mathcal{C}}) = P(g_{e_{\mathcal{C}}} \text{ is relevant})$. This probabilistic model is learned from training samples using kernel logistic regression as presented in [3].

Solving for the MAP criterion:

$$\hat{e}_{\mathcal{C}} = \arg \max_{e_{\mathcal{C}} \in \mathcal{L}^{|\mathcal{C}|}} P(o_{\mathcal{C}}|e_{\mathcal{C}})P(ge_{\mathcal{C}} \text{ is relevant}) \qquad (1)$$

cannot be achieved by testing over all possible configurations (since $\mathcal{C}$ typically involves about 50 curves, there are $2^{|\mathcal{C}|}$ possible configurations). Therefore, this minimizarion is carried out in a causal manner by introducing one-by-one ring curves $c \in \mathcal{C}$. At step k, provided the current set of labeling configurations, we evaluate the likelihood of the configurations generated by adding the k^{th} ring curve in $\mathcal{C}$ once with the label “selected” and once with the label “rejected” to each configuration of the current configuration set. We then only retain the N_{max} best configurations w.r.t. likelihood values $P(e_c|o_c)$. Typicaly, N_{max} is set to 50.

4. EXPERIMENTS

For all the experiments reported in this Section, we use the same parameter setting. The external shape of the hard tissue is represented by $N_C = 500$ points, and smoothed by a Gaussian kernel of variance 0.01. The extraction of elementary ring segments is performed for $N_{SL} = 75$ local axis uniformly sampled. The angular sector used for each local template is $\Delta\theta_{SL} = \pi/90$. Concerning the Bayesian labeling of the set of extracted ring curves, the threshold ν_1 is set to $\pi/8$ and β to 10.

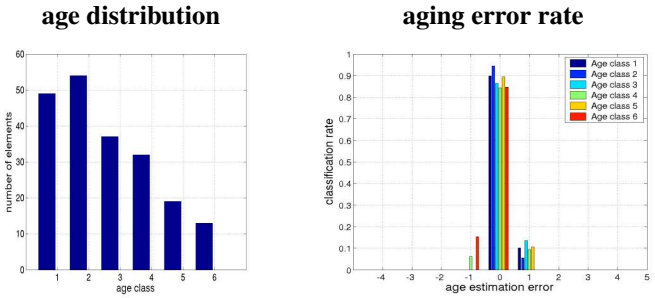

Fig. 6. *Age estimation errors for the test set of 200 images of Plaice otoliths.*

4.1. Extraction and interpretation examples

We first report in Fig.4 three examples of the extraction of meaningful ring curves within images of biological hard tissues: a plaice otolith, the shell of a bivalve seashell, and the section of a tree trunk. All these images share common characteristics in terms of rather concentric ridge and valley structures associated to a growth-based modulation. As expected, the proposed template-based growth-adapted scheme extracts meaningful ring curves mainly corresponding to the actual growth rings.

For validation purposes, the emphasis is given to fish otoliths. Among the different kinds of biological hard tissues, they provide representative examples in terms of complexity of the interpretation task. This will also enable the quantitative comparison to previous work [5, 9, 10]. Our evaluation set is formed by 400 hundred plaice otoliths from the fourth quarter collected by Ifremer at the fish-market of Boulogne/Mer in 1993 and 2000. Half of the dataset is used to train the *a priori* growth, whereas the other half is used for the evaluation of our approach.

To illustrate the behavior of the different stages of our approach, we provide in Fig.5 the results for a six year old plaice otolith (seven translucent rings). Relevant ridge curves are extracted, and the selected interpretation is the same as the expert one. This example was chosen to illustrate the ability of our approach to extract ridge and valley structures close to the otolith edge thanks to the growth-adapted filtering used within the semi-local template framework.

Concerning computational time, our approach runs under Matlab 7. The extraction of 2D ring curves runs in about 30 seconds on a 2.4GHz Pentium IV, whereas the Bayesian labeling needs a few seconds.

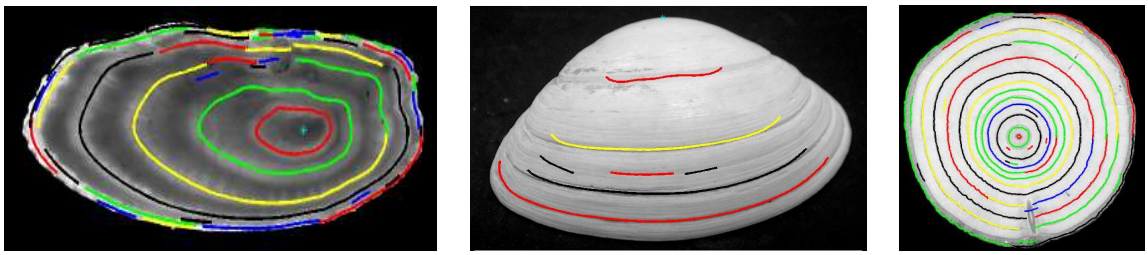

Fig. 4. *Examples of extraction of meaningful ring structures within images of biological hard tissues depicting growth ring structures. The first image displays an application to a fish otolith, the second one to the shell of a bivalve seashell and the third one to the section of a tree trunk.*

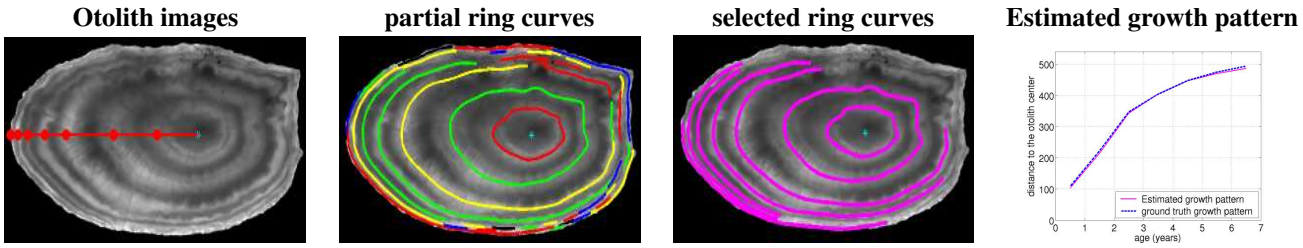

Fig. 5. *Interpretation of an image of a 6-year-old plaice otolith: the first image depicts the otolith images and the associated expert interpretations, the second one the extracted ridge curves, the third one the curve subsets selected for age and growth estimation and the fourth one the estimated growth patterns compared to the ground truth ones. For each example, the ground truth is provided by the interpretation of an expert in Plaice otolith reading.*

4.2. Quantitative evaluation

Using the second half of the collected set of plaice otoliths (i.e., a database of 200 otoliths), we have carried out a quantitative evaluation of the proposed approach. The age distribution of this database is reported in Fig.6. This is representative of the age distributions estimated from commercial landings, where samples of age group six and less usually represent more than 90% of the total. Otoliths older than six can also be found. However, the number of samples for age groups greater than six is not sufficient to learn a relevant growth model. Consequently, they were not considered during our evaluation.

The whole set of otoliths was interpreted by an expert in plaice age readings. We use these interpretations as the ground-truth to compute the class-by-class and overall age estimation errors. These results are given in Fig.6. The agreement rate is comprised between 84% for age group five and 94% for age group two. The overall agreement rate of 89% shows that the proposed approach outperforms previous work, since the maximum overall agreement rate for the different 2D methods evaluated in [5] was below 80% for a similar test set. These results stress the need for the Bayesian interpretation stage combined to the extraction of candidate ring curves. Besides, for the whole set of 200 otoliths, the estimation error is never greater than one. In addition, the obtained results are in the range of the inter-expert agreement rates, what validates the interest of the proposed approach as an operational aging tool.

5. REFERENCES

[1] F. Cao. Good continuations in digital image level lines. In *Proc of IEEE Int. Conf. on Computer Vision, ICCV'03*, pages 440–447, Nice, France, Oct. 2003.

[2] B. Chalmond, R. Azencott, and F. Colefy. Markov fusion of a pair of noisy images to detect intensity valleys. *Int. Jal of Comp. Vis.*, 16:135–145, 1995.

[3] R. Fablet. Statistical learning applied to computer-assisted fish age and growth estimation from otolith images. *Mar. and Fresh. Res.*, 2004. Submitted.

[4] R. Fablet and N. Le Josse. Automated fish age estimation from otolith images using statistical learning. *Jal of Fish. Res.*, 2004. In press.

[5] A. Guillaud, A. Benzinou, H. Troadec, V. Rodin, and J. Le Bihan. Autonomous agents for edge detection and continuity perception on otolith images. *Im. and Vis. Comp.*, 20(13-14):955–968, 2002.

[6] G. Guy and G. Medioni. Inferring global perceptual contours from local features. *Int. Jal of Comp. Vis.*, 20(1):113–133, 1996.

[7] T. Lindeberg. Edge detection and ridge detection with automatic scale selection. *Int. Jal of Comp. Vis.*, 30(2):117–154, 1998.

[8] A.K. Morison, S.G. Robertson, and D.C. Smith. An integrated system for production fish aging: image analysis and quality insurance. *North Am. Jal of Fish. Man.*, 18:587–598, 1998.

[9] H. Traodec, A. Benzinou, V. Rodin, and J. Le Bihan. Use of deformable templates for otolith 2D growth ring detection by digital image processing. *Jal of Fish. Res.*, 46(1-3):155–163, 2000.

[10] H.C. Welleman and F. Storbeck. Automatic ageing of Plaice otoliths by means of image analysis. In D.H. Secor, J.M. Dean, and S.E. Campana, editors, *Recent developments in Fish Otolith Research*, pages 271–282. Univ. of South Carolina Press, 1995.